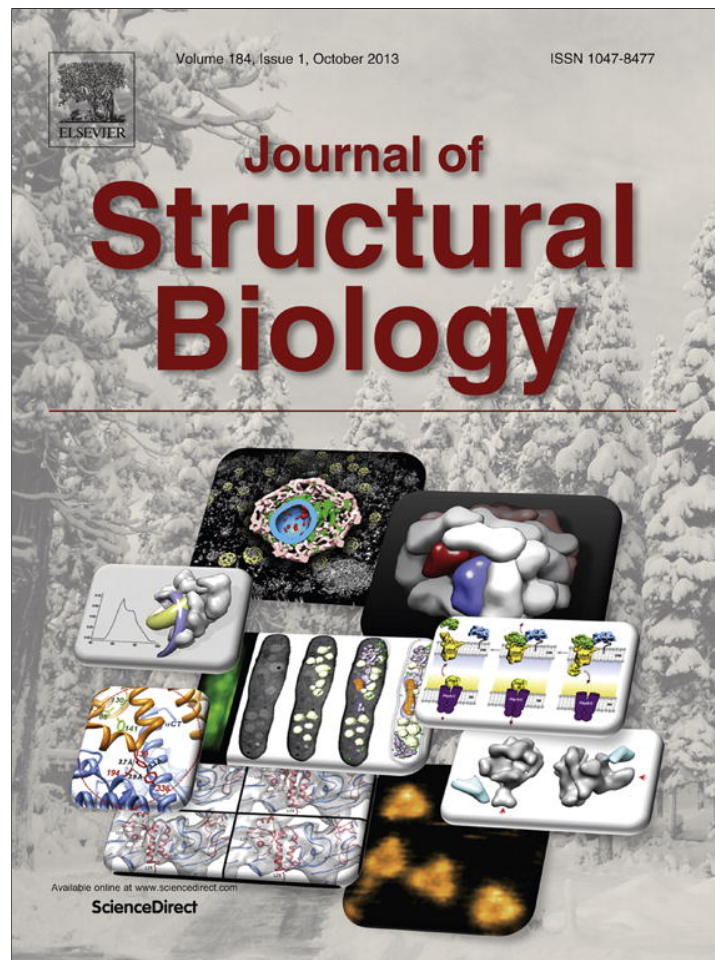


Provided for non-commercial research and education use.
Not for reproduction, distribution or commercial use.



This article appeared in a journal published by Elsevier. The attached copy is furnished to the author for internal non-commercial research and education use, including for instruction at the authors institution and sharing with colleagues.

Other uses, including reproduction and distribution, or selling or licensing copies, or posting to personal, institutional or third party websites are prohibited.

In most cases authors are permitted to post their version of the article (e.g. in Word or Tex form) to their personal website or institutional repository. Authors requiring further information regarding Elsevier's archiving and manuscript policies are encouraged to visit:

<http://www.elsevier.com/authorsrights>



Contents lists available at SciVerse ScienceDirect

Journal of Structural Biology

journal homepage: www.elsevier.com/locate/yjsbi

Role of trimer–trimer interaction of bacteriorhodopsin studied by optical spectroscopy and high-speed atomic force microscopy



Hayato Yamashita^{a,1,3}, Keiichi Inoue^{b,3}, Mikihiro Shibata^{a,2}, Takayuki Uchihashi^{a,c}, Jun Sasaki^b, Hideki Kandori^b, Toshio Ando^{a,c,*}

^a Department of Physics, Kanazawa University, Kakuma-machi, Kanazawa 920-1192, Japan

^b Department of Frontier Materials, Nagoya Institute of Technology, Showa-ku, Nagoya 466-8555, Japan

^c Bio-AFM Frontier Research Center, Kanazawa University, Kakuma-machi, Kanazawa 920-1192, Japan

ARTICLE INFO

Article history:

Available online 24 February 2013

Keywords:

High-speed atomic force microscopy
Bacteriorhodopsin
Trimer
Point mutation
Low-temperature UV–visible spectroscopy
Proton pumping efficiency

ABSTRACT

Bacteriorhodopsin (bR) trimers form a two-dimensional hexagonal lattice in the purple membrane of *Halobacterium salinarum*. However, the physiological significance of forming the lattice has long been elusive. Here, we study this issue by comparing properties of assembled and non-assembled bR trimers using directed mutagenesis, high-speed atomic force microscopy (HS-AFM), optical spectroscopy, and a proton pumping assay. First, we show that the bonds formed between W12 and F135 amino acid residues are responsible for trimer–trimer association that leads to lattice assembly; the lattice is completely disrupted in both W12I and F135I mutants. HS-AFM imaging reveals that both crystallized D96N and non-crystallized D96N/W12I mutants undergo a large conformational change (i.e., outward E–F loop displacement) upon light-activation. However, lattice disruption significantly reduces the rate of conformational change under continuous light illumination. Nevertheless, the quantum yield of M-state formation, measured by low-temperature UV–visible spectroscopy, and proton pumping efficiency are unaffected by lattice disruption. From these results, we conclude that trimer–trimer association plays essential roles in providing bound retinal with an appropriate environment to maintain its full photo-reactivity and in maintaining the natural photo-reaction pathway.

© 2013 Elsevier Inc. All rights reserved.

1. Introduction

Intermolecular interactions play a pivotal role in the function of membrane proteins. Numerous membrane proteins interact with each other or other components in two-dimensional membrane environments, e.g., self-assembly into oligomers or crystals (Essen et al., 1998; Persike et al., 2001; van Huizen et al., 1999; Colom et al., 2012), receptor-mediated protein–protein interactions for signal transduction (Szidonya et al., 2008), and the membrane localization of proteins via association with lipid rafts (Simons and Ikonen,

1997). Thus, elucidating the intermolecular packing of membrane proteins is essential for understanding the structure–function relationship and the general principle of membrane protein assembly.

Bacteriorhodopsin (bR), a light-driven proton pump in *Halobacterium* (*H.*) *salinarum* (Oesterhelt and Stoeckenius, 1971), is one of the best-characterized transmembrane proteins (see reviews: Haupt et al., 1999; Lanyi, 2004; Lanyi, 2006; Hirai et al., 2009). Under the native condition, bR forms trimers that assemble into a two-dimensional hexagonal lattice called the purple membrane (PM) (Blaurock and Stoeckenius, 1971). Previously, numerous structural studies of bR in PM were performed under unphotolyzed (Sass et al., 2000) or frozen activated (Luecke et al., 1999; Subramaniam and Henderson, 2000; Vonck, 2000; Lanyi and Schobert, 2003; Hirai and Subramaniam, 2009) states. Recently, by means of high-speed atomic force microscopy (HS-AFM) (Ando et al., 2001; Ando et al., 2008), light-induced conformational changes of bR have been visualized in real-time and real-space (Shibata et al., 2010; Shibata et al., 2011). HS-AFM movies have revealed that the E–F inter-helical loop of each bR monomer moves outwards from its trimer center upon photo-excitation from the ground state to the M_N state, which results in contact among three nearest-neighbor bR monomers, each belonging to a different adjacent trimer. This triad of

Abbreviations: AFM, atomic force microscopy; bR, bacteriorhodopsin; PM, purple membrane; HPLC, high-performance liquid chromatography; HS-AFM, high-speed atomic force microscopy; WT, wild-type.

* Corresponding author at: Department of Physics, Kanazawa University, Kakuma-machi, Kanazawa 920-1192, Japan. Tel.: +81 76 264 5663; fax: +81 76 264 5739.

E-mail address: tando@staff.kanazawa-u.ac.jp (T. Ando).

¹ Present address: Department of Pharmacology, School of Medicine, Keio University, Tokyo, Japan.

² Present address: Department of Neurobiology, Duke University Medical Center, North Carolina, USA.

³ These authors contributed equally to this work.

nearest-neighbor monomers is designated the 'trefoil'. This bR–bR interaction within a trefoil, which occurs under a relatively strong light illumination, engenders both positive and negative (i.e., bipolar) cooperative effects in decay kinetics; an early activated monomer within a trefoil decays more slowly, whereas the latest activated monomer within a trefoil decays faster than that in the case in which only one monomer within a trefoil is activated (and hence no bR–bR interaction occurs) under weak light illumination. However, because of bipolar cooperative effects, the overall turnover rate is maintained over a wide range of light intensities (Shibata et al., 2010).

An HS-AFM observation has also showed that a bR trimer occasionally rotates around a pivotal point at the interface between dense crystal and non-assembled areas of PM, suggesting the presence of specific inter-trimer interaction sites at the outer rim of a bR trimer (Yamashita et al., 2009). This is consistent with the result obtained from a neutron diffraction study suggesting that some of the aromatic residues (W10, W12, Y131, and F135) located vertically no farther than 5 Å into the extracellular side of the membrane and laterally at the outer rim of a trimer are involved in lattice formation (Weik et al., 1998). This suggestion is derived from the measured glycolipid distribution in the membrane and the possible hydrophobic stacking between aromatic side chains and carbohydrates (Qian et al., 1995) as well as from the close proximity between W10–W12 and Y131–F135 in the bR assembly. However, a more definite and specific identification of amino acids responsible for lattice formation has not been performed ever since.

In the present study, we specified amino acid residues involved in trimer–trimer association by preparing five bR mutants in which isoleucine was substituted for the aromatic residues mentioned above or phenylalanine was substituted for W12. HS-AFM observations of these mutants showed that the trimers of bR mutants (W12I and F135I) do not assemble and instead rapidly diffuse in the membrane. Furthermore, the HS-AFM observation of the D96N/W12I bR mutant revealed that lattice disruption reduces the rate of light-induced conformation change, which is proportional to light intensity. Interestingly, the spectroscopic and proton pumping assay studies, however, showed that proton pumping efficiency is unaffected by W12I mutation. Taking these results into consideration, we propose a model in which lattice disruption causes the photo-reaction pathway to branch into two: the original productive pathway and a new non-productive pathway. In the non-productive pathway, no significant structural change occurs in bR and no proton is pumped out; however, the kinetics on this pathway is much faster than that on the original pathway. This model quantitatively well explains all the results obtained in this study. Thus, trimer–trimer association plays essential roles in providing bound retinal with an appropriate environment to maintain its full photo-reactivity and in maintaining the natural photo-reaction pathway.

2. Materials and methods

2.1. Plasmid constructs and site-directed mutagenesis

A template plasmid containing the *bop* gene (1.6 kbp) cloned into the vector pGEM-T easy (Promega) was used (Shibata et al., 2007). Point mutations were introduced into the *bop* gene by PCR mutagenesis (Stratagene) as follows; W10I, Trp10 → Ile; W12I, Trp12 → Ile; Y131I, Tyr131 → Ile; F135I, Phe135 → Ile; W12F, Trp12 → Phe; D96N, Asp96 → Asn; and D96N/W12I, Asp96 → Asn and Trp12 → Ile. The mutated fragments were transferred to the vector pMPK69 for transformation (Peck et al., 2000), which contains a gene conferring resistance to the 3-hydro-

xy-3-methylglutaryl CoA reductase inhibitor (simvastatin, Wako) on *H. salinarum*. The resultant mutations were confirmed by sequencing the plasmids prior to the transformation of *H. salinarum*.

2.2. Transformation of *H. salinarum* and purification of bacteriorhodopsin mutants

H. salinarum strain MPK409 (Peck et al., 2000) was transformed using the plasmids described above. The transformation procedure was essentially as described previously (Cline and Doolittle, 1987). Briefly, 10 mL of cells in the early logarithmic growth phase was collected by centrifugation (6000g, 10 min) and resuspended in 500 µL of a spheroplasting solution to facilitate plasmid DNA transfection into the cells. 200 µL-aliquots of the suspension were added to 10 µL of 0.5 M EDTA in a spheroplasting solution and gently mixed. After 20 min, 15 µL of a plasmid DNA solution was added, and the resulting solution was incubated for 5 min. To this solution, an equal volume (225 µL in this case) of 60% polyethylene glycol 600 in a spheroplasting solution was added; the solution obtained was mixed gently by back and forth tilting of the tube. After 20 min of additional incubation, 10 mL of a regeneration salt solution containing 15% sucrose was added. Cells were pelleted by microcentrifugation at 5000 rpm for 20 min, and 10 mL of a regeneration salt solution was again added to the resultant pellet. After incubation for 24 h at 37 °C, 100-µL samples were spread on agar plates containing 15% sucrose and 10 µg/mL simvastatin. After 10 days of incubation at 37 °C, purple colonies were picked and grown in a complex culture medium with 10 µg/mL simvastatin. After incubation for 24 h at 37 °C, 100-µL samples were spread on agar plates containing 250 µg/mL 5-fluoroorotic acid (Wako). After a week of incubation, purple colonies were picked and grown again in a complex culture medium containing 50 µg/mL uracil, as uracil cannot be synthesized by the transformed cells lacking the *URA3* gene coding for orotidine-5-monophosphate decarboxylase that converts 5-fluoroorotic acid into toxic 5-fluorouracil. The purple membranes were isolated and purified by a usual method (Oesterhelt and Stoebenius, 1974). As W12I, F135I and D96N/W12I do not form 2D crystals in the native membrane, the bottom layer containing the highest bR content was collected by sucrose density gradient centrifugation. After removing sucrose by sedimentation, the pellets were suspended in a solution (Buffer-A) containing 10 mM phosphate (pH 7.0) and 300 mM KCl. For AFM observation, the samples were diluted to ~0.1 mg/mL in Buffer-A.

2.3. HS-AFM observation

The laboratory-built HS-AFM apparatus used in this study is similar to that previously reported (Ando et al., 2008). The detailed procedures towards HS-AFM imaging are reported elsewhere (Uchihashi et al., 2012). HS-AFM images were acquired in the tapping mode. To detect cantilever deflection, we used an optical beam deflection detector equipped with an infrared laser (980 nm) to avoid exciting bR. The laser beam was focused onto a small cantilever using a ×50 objective lens. The cantilever with a spring constant of ~0.2 N m⁻¹ (Olympus) is 6–7 µm long, 2 µm wide and 90 nm thick. Its resonant frequency and quality factor in an aqueous solution are ~1 MHz and ~2, respectively. An amorphous carbon tip was grown on the original cantilever tip by electron beam deposition. Tip length was adjusted to ~1 µm. The tip apex was sharpened by plasma etching under argon gas (~4 nm in radius). For HS-AFM imaging, the cantilever free-oscillation amplitude was set at ~1 nm, and the set-point amplitude was set at 90% of the free-oscillation amplitude. A sample stage made of quartz glass was placed on the z-scanner, and a 1.5-mm-diameter mica disk was glued onto the sample stage. A 2-µL sample droplet

was deposited on the freshly cleaved mica surface and then incubated for 3 min. In the HS-AFM observation of the non-assembled bR samples, bR was chemically anchored on a substrate surface to avoid its rapid diffusion. For this purpose, we used a mica surface treated with 3-aminopropyltriethoxysilane (aminosilane) (Shin-Etsu Silicones) and then with glutaraldehyde (Nacalai tesque); first, 0.1% aminosilane solution in water was placed on a freshly cleaved mica surface and incubated for 3 min. After rinsing with water, a 0.1% glutaraldehyde solution was placed on the mica surface and incubated for 3 min. After rinsing the surface with water, a sample droplet was placed on the mica surface and incubated for 3 min. HS-AFM measurement was performed under Buffer-A solution at room temperature.

For the photo-excitation of bR samples, a green laser (532 nm) was irradiated through the $\times 50$ objective lens. The intensity measured at the exit of the objective lens was varied in the range of 0.02–1 μ W.

The center of mass of each imaged bR monomer was analyzed as reported previously (Shibata et al., 2010). First, a whole AFM image was segmented into each monomer region using a watershed algorithm. Second, the grayscale of each segment was digitized using a threshold determined by a fuzzy-entropy algorithm. At each segment, an ensemble of pixels with grayscales above the threshold was defined as a monomer region (region of interest, ROI). Finally, the center of mass of a monomer is calculated using the X, Y and Z coordinates of pixels in the ROI.

2.4. UV-visible spectroscopy

The absorption spectra of bR mutants were measured at room temperature using a UV-visible spectrometer UV-1700 (Shimadzu). The bR samples were suspended in a solution containing 10 mM phosphate (pH 7.0) and 300 mM KCl.

2.5. HPLC analysis

A high-performance liquid chromatography (HPLC) analysis of the composition of retinal isomers was conducted as previously described (Shimono et al., 2001). The HPLC apparatus was equipped with a silica column (6.0 ϕ \times 150 mm³; YMC-Pack SIL). The solvent composed of 12% (v/v) ethyl acetate and 0.12% (v/v) ethanol in hexane was supplied at a flow rate of 1.0 mL/min. The extraction of retinal oxime from the bR samples was carried out in hexane after denaturation by methanol and 500 mM hydroxylamine at 4 °C. The molar composition of retinal isomers was calculated from the peak area corresponding to each retinal isomer in the HPLC elution patterns. The assignment of the peaks was performed as reported previously (Sudo et al., 2011). Three independent measurements were averaged.

2.6. Low-temperature UV-visible spectroscopy

The photo-reaction efficiency of D96N/W12I bR relative to D96N bR was estimated from the changes in the UV-visible absorption spectra of both samples upon light illumination at 210 K. For this estimation, the absorption spectra were measured using a UV-visible spectrometer (V-550, JASCO, Japan) equipped with a cryostat (DN1704, Oxford Instruments, UK). The sample was placed on a BaF₂ window of 18 mm diameter, and a dried PM film was hydrated by placing a drop of H₂O next to the film. The hydrated film on the BaF₂ window was covered with another window and placed in the cryostat sample cell in the spectrometer. The photo-reaction of the sample was initiated by the illumination of 580 \pm 10 nm light from a halogen-tungsten lamp (1000 W) (HILUX-H130, Rikagaku Seiki, Japan) for total 300 s at 210 K, and the spectral changes were measured at 10-s intervals. The initial

absorbance of both samples was adjusted to 0.6 at 580 nm to make the number of absorbed photons equivalent. The photo-reaction rate of D96N/W12I bR relative to that of D96N bR was estimated by the comparison of the magnitudes of absorption change (corresponding to the accumulation of M-intermediate) under identical illumination conditions.

2.7. Proton pumping activity assessment

H. salinarum strain MPK409 cells expressing either wild-type (WT) bR or W12I bR were grown up to the stationary phase (>1 week) in a complex culture medium at 37 °C with aeration and illumination. 100 mL of the culture was washed by centrifugation at 5000 rpm followed by the suspension of the cell pellet in a basal salt solution. After repeating the wash cycle three times, the cell pellet was suspended in 10 mL of a basal salt solution. The cell suspension was then transferred to a glass container whose temperature was regulated by circulating water adjusted at 20 °C. The sample was stirred throughout the equilibration and recording. Illumination light was provided by a 1000 W halogen-tungsten lamp output (HILUX-H130, Rikagaku Seiki, Japan) directed to the sample through a yellow cutoff filter (Y52, Toshiba, Japan). The pH of the sample was measured with a pH probe (9621-10D, HORIBA, Japan) and a pH meter (F-55, HORIBA, Japan). The pH changes occurring in the medium during bR photoactivation were calibrated by pH changes induced upon the addition of 5 μ L of 100 mM HCl to the cell suspension (50 μ M in final concentration).

In the above measurement of pH change, the observed pH change was calibrated by the amount of bR in each cell suspension. To determine the amount of bR, 10 mL of the sample was disrupted by sonication. The membrane fraction was isolated according to the standard procedure (Oesterhelt and Stoeckenius, 1974) and suspended in 2 mL of 50 mM Tris-HCl at pH 7.5. The amount of WT bR in the solution was assessed from the change in the absorption spectrum of bR caused by complete photobleaching. The photobleaching was carried out in the presence of 250 mM NH₂OH under light illumination for 10 min at ambient temperature. The light was provided in the same way as in the pH measurement described above. In WT bR, the molar extinction coefficient of 63,000 M⁻¹ cm⁻¹ at 570 nm was used for estimating molar content. To obtain the amount of W12I bR whose molar extinction coefficient is unknown, the change in its absorption at 350 nm caused by complete photobleaching was compared with that of WT bR because the absorption at 350 nm is proportional to the amount of retinal oxime produced by photobleaching.

3. Results and discussion

3.1. High speed AFM observation of bR mutants

Fig. 1A shows a schematic of the bR lattice assembly constructed from the PDB (1BRR) structure of bR trimers (Essen et al., 1998). The positions of W12 and F135 are highlighted by the white and light-blue spheres, respectively. The measurement of glycolipid distribution in PM by previous neutron diffraction studies suggested that some of the aromatic residues (W10, W12, Y131, and F135), which locate vertically no farther than 5 Å into the extracellular side of the membrane and laterally at the outer rim of the trimer, participate in inter-trimer association (Weik et al., 1998). Our previous high-resolution AFM images also suggest that the trimer-trimer association sites locate at or near the W12 residue (Yamashita et al., 2009). To identify amino acid residues responsible for inter-trimer association more specifically, we constructed five bR mutants (W10I, Y131I, W12I, F135I, and W12F).

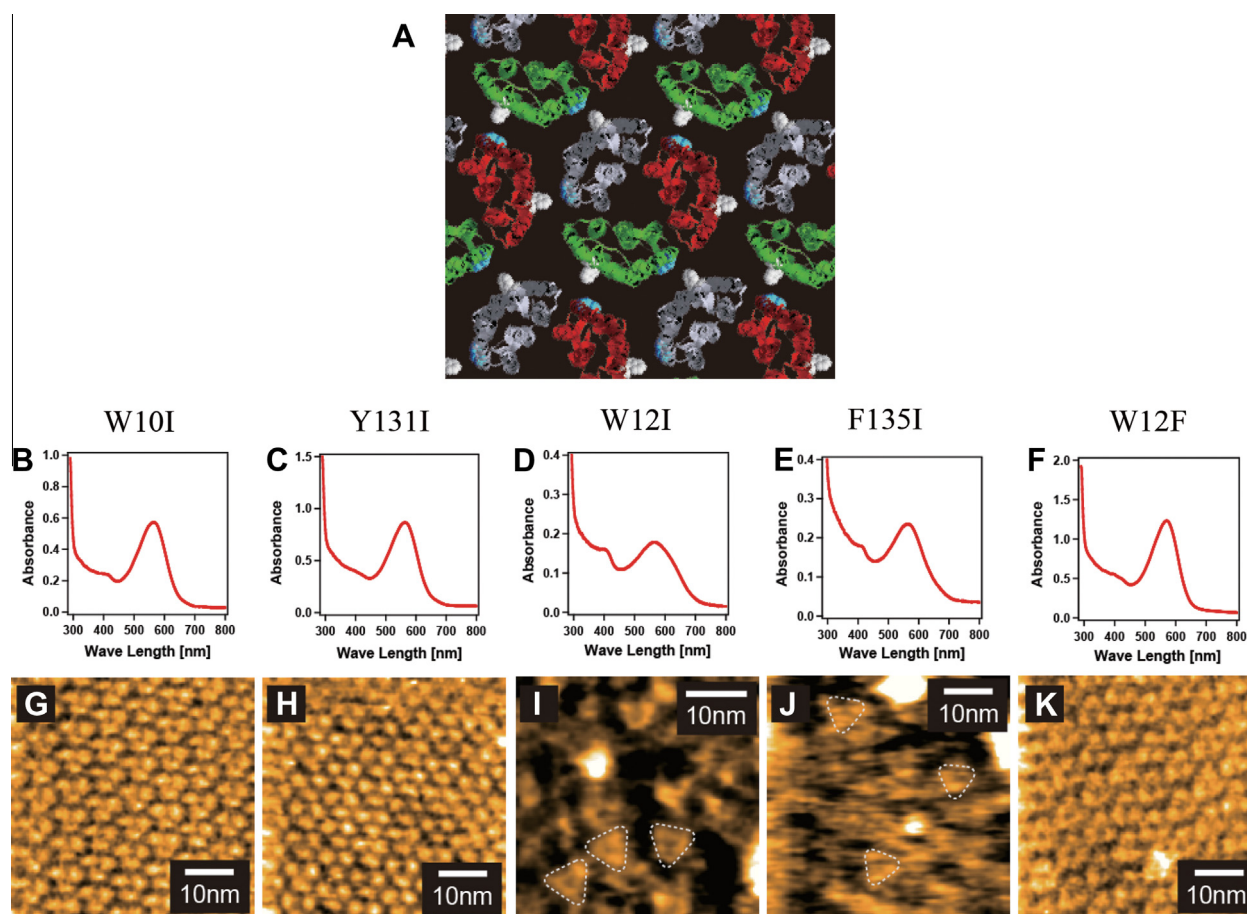


Fig. 1. (A) Schematic of bR lattice assembly (PDB 1BRR). The positions of W12 and F135 in the bR model are indicated by the white and light-blue spheres, respectively. (B–F) Absorption spectra of prepared bR mutants. (G–K) HS-AFM images of cytoplasmic surfaces of bR mutants. Images in G, H and K clearly show a packed arrangement of bR molecules. bR trimers are arranged in a hexagonal lattice with unit cell dimensions of 62 Å. Imaging rates: (G, H and K) 1 frame/s, (I and J) 3 frames/s. Z-scales: (G) 2.0 nm, (H) 2.4 nm, (I) 7.3 nm, (J) 4.0 nm, (K) 1.6 nm.

Fig. 1B–F shows the absorption spectra of the PM samples, each containing one of the five bR mutants. All of these spectra show the absorption bands around 550 nm, indicating that all mutants have a light sensitive retinal chromophore. AFM images of these bR mutants are shown in Fig. 1G–K. As can be seen in these AFM images, the W10I and Y131I mutants form a lattice assembly (Fig. 1G and H). The configuration of these lattices is identical to that of WT bR reported previously (Yamashita et al., 2009). In contrast, the lattice assembly is not seen in the AFM images of the W12I and F135I mutants (Fig. 1I and J), but some isolated trimers are seen, as indicated by dotted triangles in the images. The isolated trimers quickly diffused within the native membrane (see Movie S1 in Supporting Materials). These results indicate that both W12 and F135 residues play an essential role in assembling bR trimers (see Fig. 1A). On the other hand, the W12F mutant forms a lattice assembly, as shown in Fig. 1K. This indicates that aromatic residues at positions 12 and 135 associate with each other possibly through a hydrophobic stacking interaction mediated by the sugar moieties of glycolipids contained in the membrane (Qian et al., 1995; Weik et al., 1998).

3.2. Light-induced conformational change of bR in isolated trimer

We have recently succeeded in visualizing the light-induced conformational change of the D96N bR mutant (Shibata et al., 2010) using HS-AFM. While the wild type completes the photocycle within ~10 ms, this mutant does it within ~10 s at pH 7 but retains its proton pumping ability. This long photocycle facilitates the HS-AFM

observation of the photo-induced conformational changes of bR. To investigate the conformational change of bR in isolated trimers under light illumination, the mutation D96N was introduced to W12I bR. D96N/W12I bR also did not assemble into a lattice (Fig. 2B). Since non-assembled bR trimers diffuse on a bare mica surface too rapidly to be imaged even by HS-AFM, D96N/W12I bR trimers were immobilized on a mica surface chemically modified with aminosilane and glutaraldehyde (Fig. 2A). Fig. 2B shows the non-assembled bR trimers immobilized on the mica surface. Fig. 2C shows successive AFM images of a D96N/W12I trimer, captured at 2 frames/s (also see Movie S2 in Supporting Materials). Under green light illumination, bR molecules in the trimer appeared to move outwards from the trimer center owing to the outward movement of the corresponding E–F loops (compare the image at 0 s with those at 1–4 s in Fig. 2C); they subsequently returned back to their initial positions within a few seconds after light was switched off. However, we noticed the presence of partially inactive trimers; one or two bR molecules within a trimer did not exhibit discernible outward displacement even under long illumination (~35% of the examined bR molecules). The presence of partially inactive trimers was in contrast to the case of assembled D96N bR trimers where illuminated molecules mostly appeared to move outwards. Fig. 2D shows the displacement of the center of mass as a function of time for three bR monomers within a full-cycle D96N/W12I trimer (M1–M3 in Fig. 2D). The intermediate state of D96N with the excited conformation has been designated M_N (Kamikubo et al., 1996; Sasaki et al., 1992) because it exhibits an outward tilt of helix F similar to

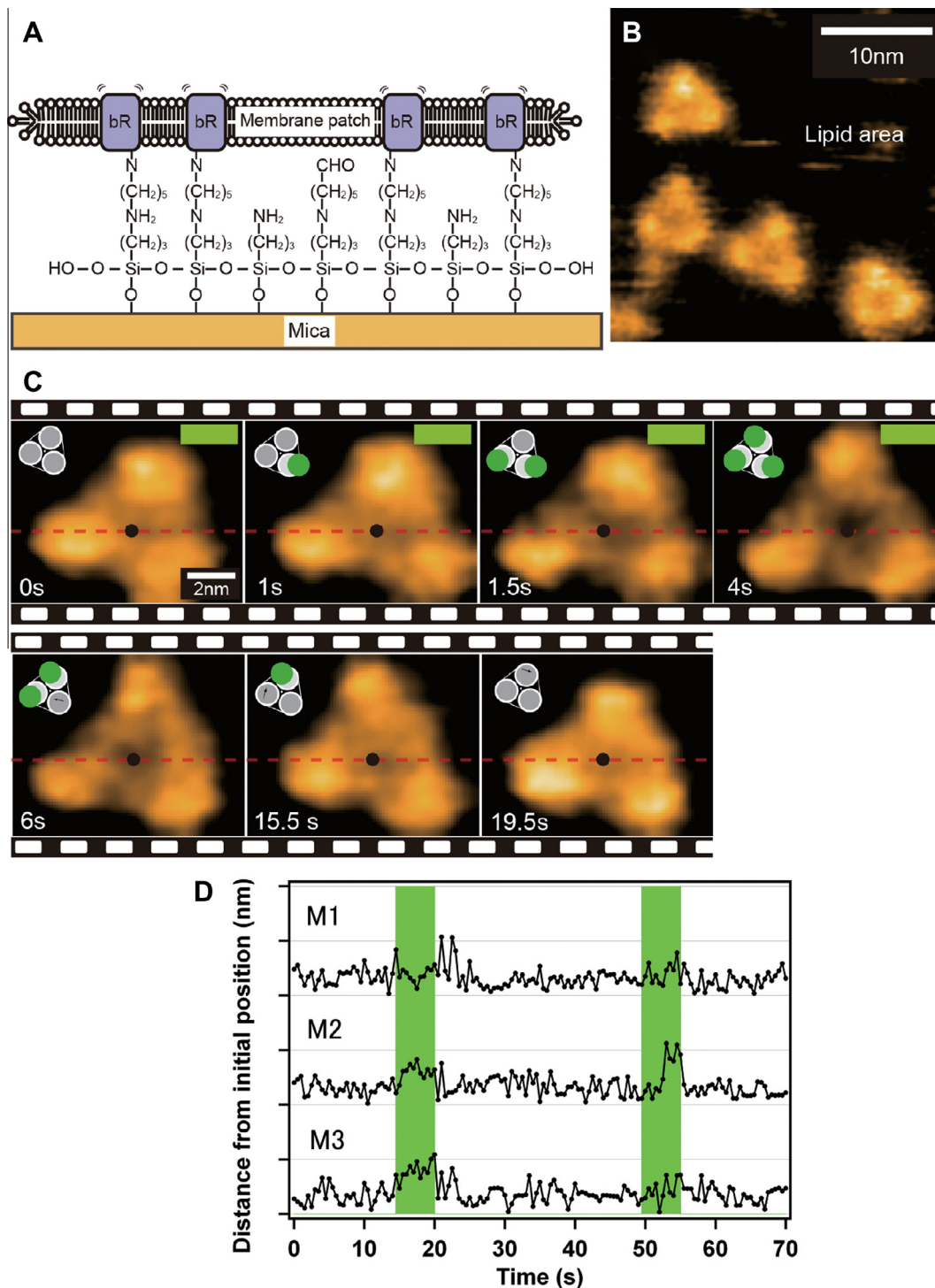


Fig. 2. (A) Schematic of anchoring bR onto chemically modified mica surface. (B) HS-AFM image of D96N/W12I bR trimers anchored on mica substrate. (C) Clips of successively captured HS-AFM images of bR trimer anchored on substrate. The green bars indicate the illumination of 532-nm green light of 0.2 μ W. The insets are schematic illustrations of the observed bR conformations. The gray and green circles indicate the conformations of bR monomers in the ground and excited states, respectively. Imaging rates: (B) 1 frame/s, (C) 2 frames/s. Z-scales: (B) 3.7 nm, (C) 1.6 nm. (D) Displacement of the center of mass as a function of time for three bR monomers (M1–M3) within a full active D96N/W12I trimer. The green regions show periods of green light illumination (532 nm).

that of the N state of WT (Vonck, 1996), while the Schiff-base is still deprotonated like the precedent M state owing to the absence of the proton donor residue (Asp96) for the Schiff base. The conformational change is reproducible throughout the repeated dark-illumination cycles (Movie S2). The observed behaviors of the double mutant are similar to those observed previously for the D96N mutant (Shibata et al., 2010), except for the partial presence of photo-inactive bR molecules in the D96N/W12I sample (to be discussed later).

3.3. Analysis of reaction kinetics and its comparison between D96N bR and D96N/W12I bR

We analyzed more details of the photo-induced conformational changes of bR to investigate a possible effect of lattice disruption on the photo-activated reaction kinetics. We first analyzed the time course of photo-activation under continuous light illumination. Fig. 3A shows the time courses in which the population of activated

D96N and D96N/W12I bR molecules increased after continuous illumination was started. The rise time constant of D96N/W12I bR was estimated to be $\tau = 1.9 \pm 0.06$ s, which was four fold longer than that of D96N bR ($\tau = 0.49 \pm 0.01$ s) under the same light intensity. On the other hand, as shown in Fig. 3B, the time constants of decay after light-off were almost identical for both mutants ($\tau \sim 10$ s). To rule out the possibility that the rise delay of D96N/W12I bR is caused by the anchoring of the molecules onto the chemically modified mica, we also observed D96N bR attached onto the chemically modified mica and examined the time constants in the rise and decay phases. As shown in the insets of Fig. 3A (rise phase) and Fig. 3B (decay phase), the respective time constants were essentially identical to those of D96N bR simply placed on a bare mica surface. Moreover, all the molecules under illumination appeared to move outwards. Thus, the chemical anchoring has no significant effect on the photocycle. The rise delay and the presence of inactive molecules observed with D96N/W12I bR are intrinsically caused by lattice disruption.

We previously found that the decay kinetics after the light-off of the photo-induced conformational change in D96N bR differs depending on the intensity of illuminated light (Shibata et al., 2010). When the intensity is strong ($\sim 0.5 \mu\text{W}$ at the exit of the objective lens; likewise, the light intensities indicated below are those measured at the exit of the objective lens), the decay rate of many excited molecules splits into shorter and longer ones (~ 2 s vs. ~ 13 s) relative to the rate (~ 7 s) observed with rarely excited molecules under weak illumination ($\sim 0.01 \mu\text{W}$). We concluded that this altered decay kinetics is caused by the interaction between bR molecules that are excited together not

within a trimer but within a 'trefoil'. Earlier works have also reported that the spectroscopically measured kinetics of the bR photocycle is altered depending on light intensity, and attributed the observed cooperative effects to neighboring effects within trimers (Rehorek and Heyn, 1979; Tokaji, 1993) or general crowding effects in the lattice (e.g., Varo et al., 1996). However, the cooperative effects observed in these ensemble-averaged spectroscopic measurements are not as distinct as those observed by HS-AFM, which is due likely to the bipolar nature of the cooperativity. Here, the issue of the cooperativity origin is further certified by examining the decay kinetics of D96N/W12I bR in full active trimers, as its trimers are isolated from each other in the membrane (i.e., absence of trefoil). Fig. 3C shows the decay of rarely activated D96N molecules under $0.022 \mu\text{W}$ illumination. The decay time is almost identical to that measured for D96N/W12I bR under $0.2 \mu\text{W}$ illumination (blue line in Fig. 3B; $\tau \sim 10$ s). Next, we measured the decay kinetics of activated monomers within full-active D96N/W12I trimers under stronger illumination (up to $1 \mu\text{W}$). In this measurement, we analyzed the decay kinetics separately for early-activated (red circles in Fig. 3D) and late-activated monomers (blue circles in Fig. 3D) within each D96N/W12I trimer. The separately analyzed decay time constants were almost identical ($\tau \sim 10$ s). Thus, the disruption of lattice assembly in the W12I bR mutant eliminates the light-intensity dependence of the decay kinetics observed with lattice-assembled bR, reinforcing our previous conclusion that the bipolar cooperative effects in the decay kinetics are engendered by the interaction between excited bR molecules within a trefoil (not within a trimer).

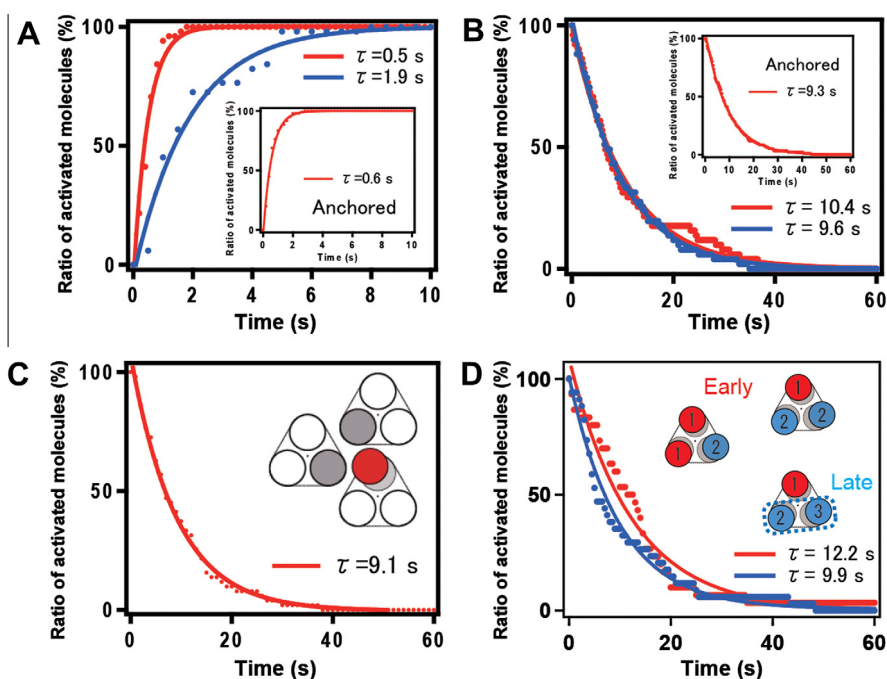


Fig. 3. (A) Time courses of accumulation of activated bR molecules detected by HS-AFM under continuous light illumination ($0.2 \mu\text{W}$). Red plots, unanchored D96N bR; blue plots, anchored D96N/W12I bR. The exponential time constants (τ) of D96N and D96N/W12I are 0.49 ± 0.01 s (total number of analyzed bR molecules, $N_T = 51$; number of different molecules analyzed, $N_m = 22$) and 1.9 ± 0.06 s ($N_T = 51$, $N_m = 16$), respectively. The inset shows the time course of the accumulation of activated bR in an anchored D96N bR sample. The exponential time constant (τ) is 0.58 ± 0.01 s. (B) HS-AFM-detected decay of activated states of unanchored D96N bR (red plots) and anchored D96N/W12I bR in full active trimers (blue plots) after light ($0.2 \mu\text{W}$) was switched off. The exponential time constant (τ) of D96N and D96N/W12I are 10.4 ± 0.10 s ($N_T = 51$, $N_m = 22$) and $\tau = 9.6 \pm 0.04$ s ($N_T = 51$, $N_m = 16$), respectively. The inset shows the decay of activated molecules for anchored D96N after light ($0.2 \mu\text{W}$) was switched off. The exponential time constant (τ) is 9.3 ± 0.04 s. (C) Decay of activated molecules for unanchored D96N after weak light ($0.022 \mu\text{W}$) was switched off. As shown in the inset, under this weak illumination, only one monomer (red circle) is excited in a trefoil, while the other two monomers (the grey circles) in the same trefoil are not excited. The exponential time constant (τ) is 9.1 ± 0.12 s. ($N_T = 51$, $N_m = 30$) (D) Decay of activated D96N/W12I bR monomers in full active trimers after strong light illumination (0.2 – $1.0 \mu\text{W}$) was switched off. The decay analysis was made separately for early-activated (red plots) and late-activated (blue plots) monomers within a trimer, as depicted by the inset illustration (red circles, early-activated molecules; blue circles, late-activated molecules). The number in these circles indicates the order in which molecules are activated. The exponential time constants (τ) for the early- and late-activated molecules are 12.2 ± 0.31 s ($N_T = 20$, $N_m = 30$) and 9.9 ± 0.18 s ($N_T = 20$, $N_m = 34$), respectively.

3.4. HPLC analysis of retinal in D96N and D96N/W12I mutants

The introduction of W12I mutation to D96N bR significantly retards the accumulation of the M_N state (outward E–F loop displacement) under continuous illumination, compared with that of the lattice-assembled D96N bR (Fig. 3A). Since the rise rate linearly increases with illumination intensity (Fig. 4A), the retardation is likely attributable to lower efficiency of the conformational change or to a smaller optical absorption cross section of the D96N/W12I mutant. The latter is, however, ruled out because the difference spectrum between the ground and 100%-excited states of D96N/W12I bR measured at low temperature (210 K) was identical to that of D96N bR, as shown in Fig. 6. Therefore, the reduced accumulation rate should be attributed to reduced efficiency of the conformational change of D96N/W12I bR. This suggests that there is a secondary pathway in which light-adsorbed D96N/W12I bR does not proceed to the M_N state (to be discussed later).

A previous AFM imaging study on native PM showed that photobleaching in the presence of hydroxylamine (Moller et al., 2000) causes bR lattice disassembly, suggesting that the removal of the retinal chromophore from bR weakens inter-trimer association. It is therefore conceivable that the loss of inter-trimer association due to W12I mutation leads to an alteration of the environment around retinal in bR, which might be involved in reduced efficiency of the conformational change of D96N/W12I bR and/or the presence of inactive molecules. To investigate this possibility, the isomeric compositions of retinal in D96N and

D96N/W12I and their quantum yields of M-formation were compared.

HPLC analysis was performed for retinal extracted from D96N bR and D96N/W12I bR in hydroxylamine. Fig. 5A shows chromatograms of retinal isomers extracted from each bR mutant under the dark- and light-adapted conditions. The retinal isomer compositions calculated from the chromatograms are summarized in Fig. 5B and Table 1. The retinal composition of D96N bR is similar to that of WT bR, that is, almost equal amounts of the all-*trans* and 13-*cis* isoforms exist in the dark, whereas the all-*trans* form predominates (~93%) over 13-*cis* after light adaptation (Pettei et al., 1977). In contrast, D96N/W12I bR shows a reduction in the degree of difference in isomeric composition between the light- and dark-adapted states (64% all-*trans* and 32% 13-*cis* in the dark-adapted state; 68% all-*trans*, 23% 13-*cis*, and trace amounts of 9-*cis* and 11-*cis* in the light-adapted state). Since the HS-AFM measurement was carried out after the light adaptation of the samples, D96N bR and D96N/W12I bR contain 93% and 68% all-*trans* retinal, respectively. Consistent with this analysis, 36.7% of the D96N/W12I bR molecules (among 147 molecules in total) observed by HS-AFM showed no discernible structural changes upon light illumination. Those molecules are considered to contain 13-*cis* retinal. However, this does not account for the retarded accumulation of the M_N state observed under constant light illumination.

3.5. Comparison between D96N bR and D96N/W12I bR by low-temperature UV-visible spectroscopy

The reduced efficiency of the conformational change of D96N/W12I bR is likely to be caused by an alteration in the photochemical reaction. Here, we compared the relative quantum yields of M-formation in D96N bR and D96N/W12I bR using UV-visible spectroscopy at low temperature (210 K) where the *M* state is absolutely stable (Sasaki et al., 1992). The hydrated films of the bR mutants were illuminated with 580-nm light. The spectra were measured after every 10-s illumination and the illumination was performed for 300 s in total (Fig. 6). The accumulation of the *M*-intermediate and the depletion of the initial state were estimated from the corresponding absorption change at 415–420 nm and 575–580 nm, respectively. The blue plots in Fig. 6C and D show the time courses of *M*-accumulation in D96N bR and D96N/W12I bR, respectively. The initial absorption peaks at the excitation wavelength (580 ± 10 nm) are the same for both samples. Therefore, both samples could be excited with the same efficiency, allowing relative comparison of the quantum yields of M-formation by directly comparing the time courses shown by the blue plots in Fig. 6C and D. The time-constant thus obtained for D96N/W12I bR ($\tau = 135$ s) was 1.5-fold smaller than that obtained for D96N bR. This means that the quantum yield of M-formation in D96N/W12I bR is reduced by ~30% compared with that in D96N bR. This reduced quantum yield should be explained by the 30% reduction in the amount of all-*trans* retinal, as revealed by the HPLC analysis. This is because bR with 13-*cis* retinal has been shown to produce no *M* state with the deprotonated Schiff-base (Gergely et al., 1994). However, this result again does not account for the retarded accumulation of the M_N state observed with D96N/W12I bR under constant light illumination.

3.6. Measurement of proton pumping efficiency

If helix-F displacement is tightly coupled with (or prerequisite for) unidirectional proton pumping, the reduced yield of the conformational change of D96N/W12I bR would result in a reduced proton pumping efficiency, compared with that of D96N bR. To address this issue, we monitored the proton pumping activity of bR molecules by measuring light-induced pH changes in the medium

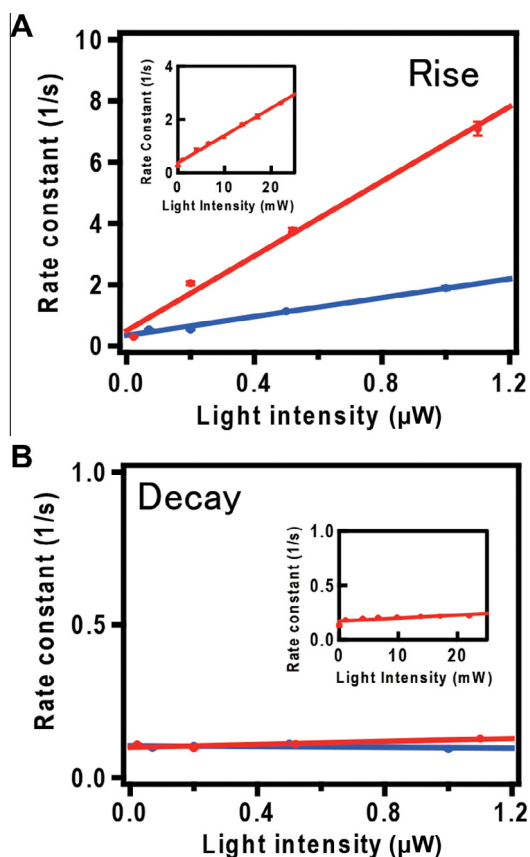


Fig. 4. Rate constants of rise (A) and decay (B) phases as functions of light intensity for D96N (red plots) and D96N/W12I (blue plots) measured by HS-AFM. These rate constants were fitted with linear functions with slopes of 6.1 ± 0.43 (red line) and 1.5 ± 0.15 (blue line) for the rise phase, and with slopes of 0.02 ± 0.01 (red line) and -0.007 ± 0.01 (blue line) for the decay phase. The insets show the rate constants of the rise (A) and decay (B) phases as functions of light intensity for D96N measured by UV-visible spectroscopy.

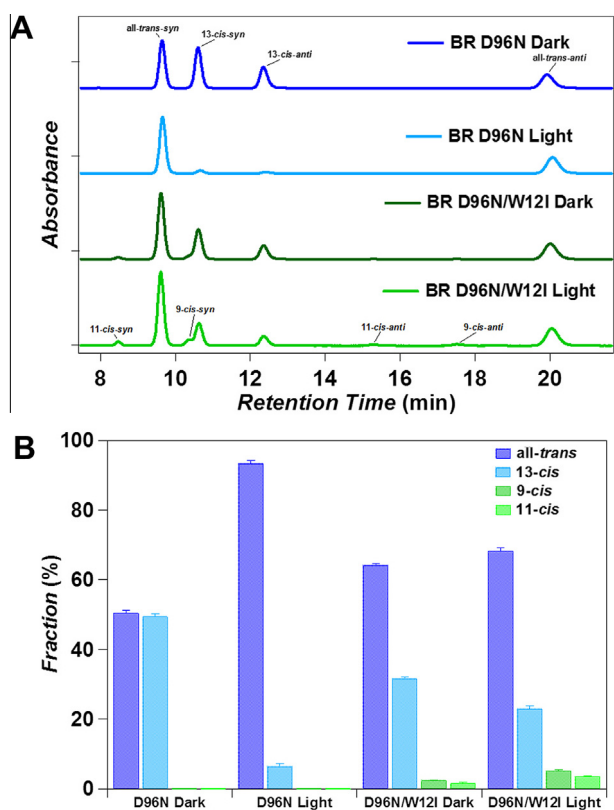


Fig. 5. Composition analysis of retinal isomers in D96N and D96N/W12I. (A) HPLC patterns of retinal extracted from D96N under dark-adapted state (blue) and after illumination of light (cyan), and from D96N/W12I under dark adapted state (dark green) and after illumination of light (light green). (B) Compositions of retinal isomers extracted from D96N and D96N/W12I under dark- and light-adapted conditions. For light adaptation, light of >500-nm wavelength was illuminated for 1 min.

in which *H. salinarum* cells expressing WT bR or W12I bR were suspended (although we should have used D96N bR and D96N/W12I bR for this assay, it was difficult to measure light-induced pH

changes because of their slow photocycle). To compare their pumping activities, light-induced changes in the proton concentration were normalized by the respective bR amounts (Fig. 7). Note that this proton pumping assay can only detect the pumping activity in the steady state because the photocycle of WT bR and W12I bR is very fast. Pumping efficiency was evaluated from the initial slope of the proton concentration increase after the onset of illumination with >500-nm light. The estimated number of protons pumped per one bR molecule was 15–18/min for both WT bR and W12I bR. Likewise, the amplitude of the proton concentration change was comparable for both samples (Fig. 7). Thus, the introduction of W12 mutation does not appear to affect proton pumping activity.

3.7. Relationship between E–F loop movement and proton pumping

The present HS-AFM and spectroscopic studies gave the following results: (i) the M_N state with an outwardly displaced E–F loop exists in the photocycle of D96N bR and D96N/W12I bR; (ii) after the start of continuous illumination, the M_N state accumulation of disassembled D96N/W12I bR occurs with a rate ~ 4 -times lower than that of assembled D96N bR; (iii) the accumulation rate of both samples linearly increases with increasing light intensity; (iv) the optical absorption cross section is very similar between D96N bR and D96N/W12I bR; and (v) the introduction of W12I mutation into WT bR does not appear to affect the proton pumping activity of bR within experimental accuracy. From these results, we propose that the photo-reaction cycle is altered by the introduction of W12I mutation, as shown in Fig. 8. The unspecified M_X state occurs first upon photo-excitation, after which the pathway branches into two: in one pathway, the M_N state is formed, while in the other pathway, the M_X state is de-excited to the ground state G. Results of numerical analysis based on this proposed reaction scheme are shown in Fig. 9. The retardation of M_N state formation by the introduction of W12I mutation (compare the red and blue solid lines in Fig. 9A) as well as the proportionality of M_N state accumulation rates to light intensity (Fig. 9B) are similar to those observed experimentally. The W12I mutation significantly reduces the ground-state depletion rate (compare the red and blue dotted lines

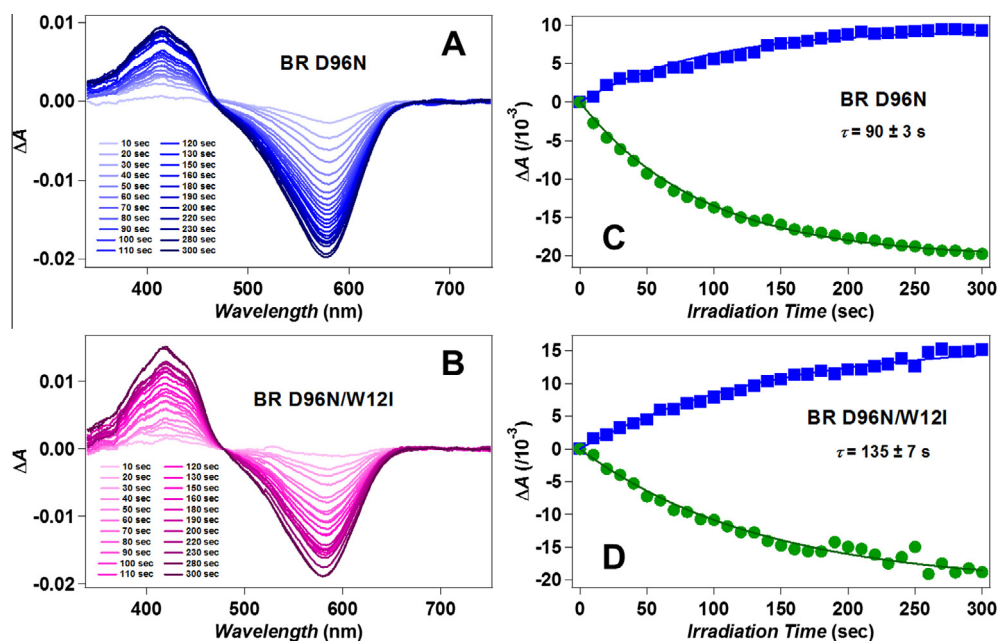


Fig. 6. Comparison of photo-reactivities between D96N and D96N/W12I. The absorption changes of (A) D96N and (B) D96N/W12I after the irradiation of light (580 ± 10 nm) are shown for the indicated irradiation durations (10–300 s). The blue squares indicate the degrees of accumulation of M intermediate monitored at 415 nm for D96N (C) and at 420 nm for D96N/W12I (D). The green circles indicate the bleaching of the initial state monitored at 577 nm for D96N (C) and at 581 nm for D96N/W12I (D).

Table 1
Compositions of retinal isomers extracted from D96N and D96N/W12I under the dark and light adapted conditions.

Retinal isomer	D96N Dark	D96N Light	D96NW12I Dark	D96NW12I Light
All-trans	50.5 ± 0.8%	93.5 ± 0.8%	64.3 ± 0.3%	68.3 ± 0.9%
13-cis	49.5 ± 0.8%	6.4 ± 0.8%	31.7 ± 0.4%	23.0 ± 0.8%
9-cis	0%	0%	2.45 ± 0.11%	5.2 ± 0.3%
11-cis	0%	0%	1.6 ± 0.2%	3.55 ± 0.19%

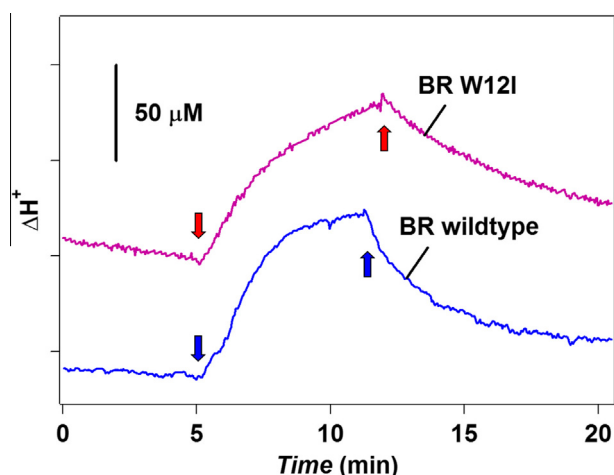


Fig. 7. Measurement of proton pumping efficiency. Proton pumping activity was monitored by the measurement of light-induced (>500 nm) pH changes in a basal salt solution in which *H. salinarum* strain MPK409 expressing either WT (blue line) or W12I (purple line) was suspended. The initial pH in the dark was ~6.5. The time points for light-on and light-off are indicated by the downward arrows and the upward arrows, respectively. The proton concentration changes were normalized by the protein concentrations and calibrated by the measurement of pH changes induced by the addition of 50 μM HCl.

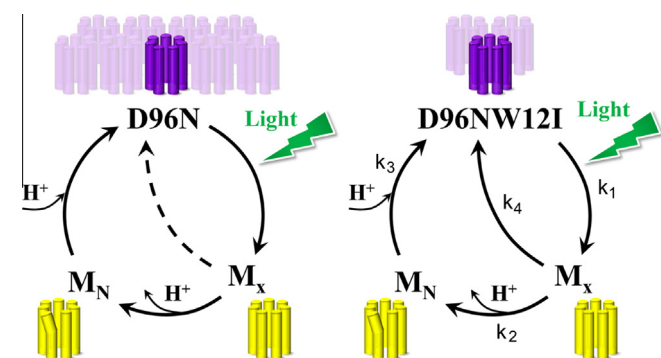


Fig. 8. Models of photocycles in D96N bR and D96N/W12I bR. Upper illustrations indicate the lattice-assembled D96N bR (left) and non-assembled D96N/W12I bR (right). The bottom schematics show the modeled photocycles in D96N bR (left) and D96N/W12I bR (right). In the photocycle of D96N bR, the presence of a direct recovery pathway from M_X with no E-F loop displacement is minor as indicated by the dashed arrow. The rate constants, k_1 , k_2 , k_3 , and k_4 , for transitions between different states are assigned as shown in the right bottom schematic.

in Fig. 9A); however, the spectroscopically measured rates are nearly identical between the D96N/W12I and D96N mutants (shown by curves with green circles in Fig. 6C and D). However, this apparent discrepancy is explained by the low temperature used for the spectroscopic measurement (i.e., the M state is completely stabilized and likewise the M_X state is likely to be stabilized to some extent at low temperature). In the steady state ($t > 10$ s), the time course of proton accumulation by D96N/W12I is only slightly lower (15%) than that by D96N (Fig. 9C). This accumulation

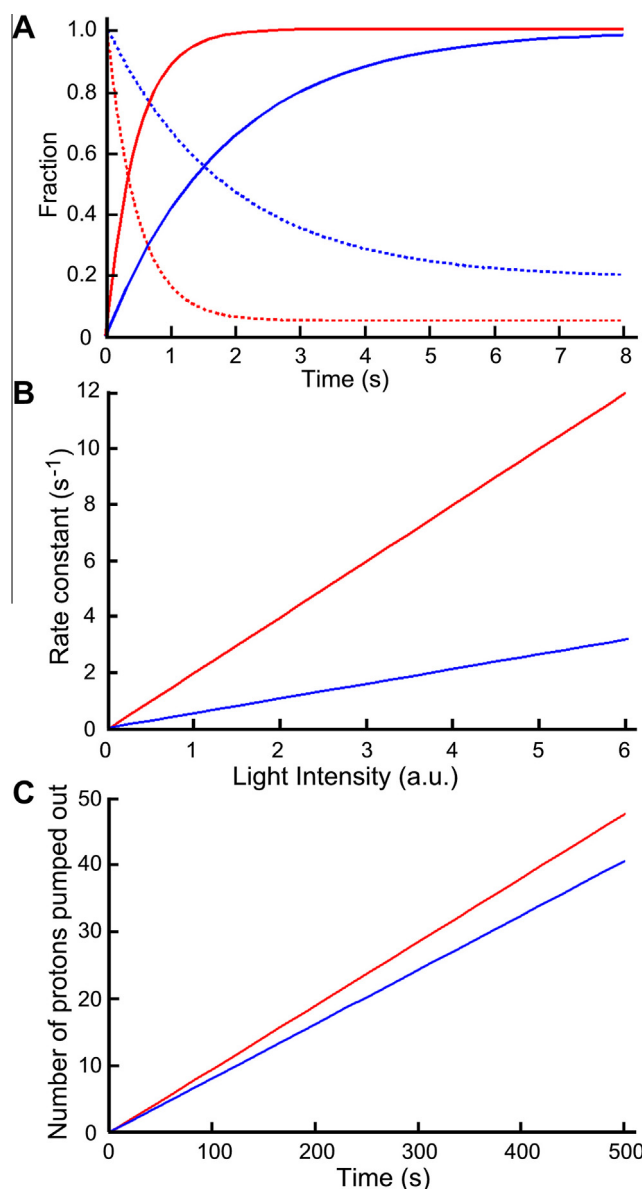


Fig. 9. Numerical analyses of M_N formation rate and proton pumping activity based on the modeled photocycle in D96N bR and D96N/W12I bR depicted in Fig. 8. (A) Time courses of M_N state accumulation (solid lines) and ground state depletion (dotted lines) for D96N bR (red lines) and D96N/W12I bR (blue lines) after continuous light illumination. The time courses of M_N state accumulation are normalized by respective saturated values. (B) Relationship of M_N state accumulation rate and light intensity for D96N bR (red line) and D96N/W12I bR (blue line). (C) Time courses of proton accumulation by D96N bR (red line) and D96N/W12I bR (blue line). Here, it was assumed that proton pumping only occurs through M_N . In the calculations of (A) and (C), the following rate constants (see Fig. 8) were used: $k_1 = 2.04 \text{ s}^{-1}$, $k_2 = 100.0 \text{ s}^{-1}$, $k_3 = 0.1 \text{ s}^{-1}$, and $k_4 = 0 \text{ s}^{-1}$ (D96N bR) or 370.4 s^{-1} (D96N/W12I bR). In the calculation of (B), the rate constant k_1 was varied from 0 s^{-1} to 12.24 s^{-1} , while the other rate constants were the same as those used for (A) and (C).

is calculated under the assumption that protons are transferred only through the M_N state. Because WT bR and W121 bR with a fast photocycle were used in the proton pumping assay, the pumping activities measured are in the steady state. Thus, the small difference of 15% seems to be within experimental error. Even if protons are pumped through the new pathway, its contribution is negligible because the fraction of the M_X state is negligible (<0.02%) according to the results of the numerical analysis based on the proposed model.

4. Conclusions

The aromatic interaction between W12 and F135 located vertically no farther than 5 Å into the extracellular side of the membrane and laterally at the outer rim of the bR trimer is responsible for inter-trimer association in the hexagonal lattice of trimers. The replacement of W with F (i.e., W12F) maintains inter-trimer association. The loss of trimer–trimer interactions in D96NW121 bR abolishes the positive and negative cooperative effects on decay kinetics as the initial ground state recovers. It also produces ~35% inactive bR molecules owing to the reduction in the amount of all-*trans* retinal. Interestingly, the loss of trimer–trimer interactions reduces the rate of photo-induced conformational change in bR (outward displacement of the E–F loop) down to a quarter, which is very likely to be caused by the branching of the photocycle into two pathways. Thus, trimer–trimer association plays essential roles in providing bound retinal with an appropriate environment to maintain its full photo-reactivity and in maintaining the natural photo-reaction pathway.

Acknowledgments

This research was supported by JST CREST (T.A.), Knowledge Cluster/MEXT Japan (T.A.), Grants-in-Aids for Scientific Research from the MEXT Japan (Nos. 15101005, T.A.; 22018012, K.I.; 19042009, T.U.; 20108014, H.K.) and a Research Fellowship of JSPS for Young Scientists (M.S.).

Appendix A. Supplementary data

Supplementary data associated with this article can be found, in the online version, at <http://dx.doi.org/10.1016/j.jsb.2013.02.011>.

References

- Ando, T., Kodera, N., Takai, E., Maruyama, D., Saito, K., et al., 2001. A high-speed atomic force microscope for studying biological macromolecules. *Proc. Natl. Acad. Sci. USA* 98, 12468–12472.
- Ando, T., Uchihashi, T., Fukuma, T., 2008. High-speed atomic force microscopy for nano-visualization of dynamic biomolecular processes. *Prog. Surf. Sci.* 83, 337–374.
- Blaurock, A.E., Stoekenius, W., 1971. Structure of the purple membrane. *Nat. New Biol.* 233, 152–154.
- Cline, S.W., Doolittle, W.F., 1987. Efficient transfection of the archaeobacterium *Halobacterium halobium*. *J. Bacteriol.* 169, 1341–1344.
- Colom, A., Casuso, I., Boudier, T., Scheuring, S., 2012. High-speed atomic force microscopy: cooperative adhesion and dynamic equilibrium of junctional microdomain membrane proteins. *J. Mol. Biol.* 423, 249–256.
- Essen, L.O., Siebert, R., Lehmann, W.D., Oesterhelt, D., 1998. Lipid patches in membrane protein oligomers: crystal structure of the bacteriorhodopsin-lipid complex. *Proc. Natl. Acad. Sci. USA* 95, 11673–11678.
- Gergely, C., Ganea, C., Varo, G., 1994. Combined optical and photoelectric study of the photocycle of 13-*cis* bacteriorhodopsin. *Biophys. J.* 67, 855–861.
- Haupts, U., Tittor, J., Oesterhelt, D., 1999. Closing in on bacteriorhodopsin: progress in understanding the molecule. *Annu. Rev. Biophys. Biomol. Struct.* 28, 367–399.
- Hirai, T., Subramaniam, S., Lanyi, J.K., 2009. Structural snapshots of conformational changes in a seven-helix membrane protein: lessons from bacteriorhodopsin. *Curr. Opin. Struct. Biol.* 19, 433–439.
- Hirai, T., Subramaniam, S., 2009. Protein conformational changes in the bacteriorhodopsin photocycle: comparison of findings from electron and X-ray crystallographic analyses. *J. Mol. Biol.* 328, 439–450.
- Kamikubo, H., Kataoka, M., Varo, G., Oka, T., Tokunaga, F., et al., 1996. Structure of the N intermediate of bacteriorhodopsin revealed by X-ray diffraction. *Proc. Natl. Acad. Sci. USA* 93, 1386–1390.
- Lanyi, J.K., 2004. Bacteriorhodopsin. *Annu. Rev. Physiol.* 66, 665–688.
- Lanyi, J.K., 2006. Review: proton transfers in the bacteriorhodopsin photocycle. *Biochim. Biophys. Acta* 1757, 1012–1018.
- Lanyi, J.K., Schobert, B., 2003. Mechanism of proton transport in bacteriorhodopsin from crystallographic structures of the K, L, M₁, M₂' and M₂' intermediates of the photocycle. *J. Mol. Biol.* 328, 439–450.
- Luecke, H., Schobert, B., Richter, H.T., Cartailler, J.P., Lanyi, J.K., 1999. Structural changes in bacteriorhodopsin during ion transport at 2 Å resolution. *Science* 286, 255–261.
- Moller, C., Buldt, G., Dencher, N.A., Engel, A., Muller, D.J., 2000. Reversible loss of crystallinity on photobleaching purple membrane in the presence of hydroxylamine. *J. Mol. Biol.* 301, 869–879.
- Oesterhelt, D., Stoekenius, W., 1971. Rhodopsin-like protein from the purple membrane of *Halobacterium halobium*. *Nat. New Biol.* 233, 149–152.
- Oesterhelt, D., Stoekenius, W., 1974. Isolation of the cell membrane of *Halobacterium halobium* and its fractionation into red and purple membrane. *Meth. Enzymol.* 31, 667–678.
- Peck, R.F., Dassarma, S., Krebs, M.P., 2000. Homologous gene knockout in the archaeon *Halobacterium salinarum* with *ura3* as a counterselectable marker. *Mol. Microbiol.* 35, 667–676.
- Persike, N., Pfeiffer, M., Guckenberger, R., Radmacher, M., Fritz, M.G., 2001. Direct observation of different surface structures on high-resolution images of native halorhodopsin. *J. Mol. Biol.* 310, 773–780.
- Pettei, M.J., Yudd, A.P., Nakanishi, K., Henselman, R., Stoekenius, W., 1977. Identification of retinal isomers isolated from bacteriorhodopsin. *Biochemistry* 16, 1955–1959.
- Qian, M., Haser, R., Payan, F., 1995. Carbohydrate binding sites in a pancreatic alpha-amylase-substrate complex, derived from X-ray structure analysis at 2.1 Å resolution. *Protein Sci.* 4, 747–755.
- Rehorek, M., Heyn, M.P., 1979. Binding of all-*trans*-retinal to the purple membrane. Evidence for cooperativity and determination of the extinction coefficient. *Biochemistry* 18, 4977–4983.
- Sasaki, J., Shichida, Y., Lanyi, J.K., Maeda, A., 1992. Protein changes associated with reprotonation of the Schiff base in the photocycle of Asp96 → Asn bacteriorhodopsin. The MN intermediate with unprotonated Schiff base but N-like protein structure. *J. Biol. Chem.* 267, 20782–20786.
- Sass, H.J., Buldt, G., Gessenich, R., Hehn, D., Neff, D., et al., 2000. Structural alterations for proton translocation in the M state of wild-type bacteriorhodopsin. *Nature* 406, 649–653.
- Shibata, M., Yoshitsugu, M., Mizuide, N., Ihara, K., Kandori, H., 2007. Halide binding by the D212N mutant of bacteriorhodopsin affects hydrogen bonding of water in the active site. *Biochemistry* 46, 7525–7535.
- Shibata, M., Yamashita, H., Uchihashi, T., Kandori, H., Ando, T., 2010. High-speed atomic force microscopy shows dynamic molecular processes in photoactivated bacteriorhodopsin. *Nat. Nanotechnol.* 5, 208–212.
- Shibata, M., Uchihashi, T., Yamashita, H., Kandori, H., Ando, T., 2011. Structural changes in bacteriorhodopsin in response to alternate illumination observed by high-speed atomic force microscopy. *Angew. Chem. Int. Ed. Engl.* 50, 4410–4413.
- Shimono, K., Ikeura, Y., Sudo, Y., Iwamoto, M., Kamo, N., 2001. Environment around the chromophore in pharaonis phorbodopsin: mutation analysis of the retinal binding site. *Biochim. Biophys. Acta* 1515, 92–100.
- Simons, K., Ikonen, E., 1997. Functional rafts in cell membranes. *Nature* 387, 569–572.
- Subramaniam, S., Henderson, R., 2000. Molecular mechanism of vectorial proton translocation by bacteriorhodopsin. *Nature* 406, 653–657.
- Sudo, Y., Ihara, K., Kobayashi, S., Suzuki, D., Irieda, H., et al., 2011. A microbial rhodopsin with a unique retinal composition shows both sensory rhodopsin II and bacteriorhodopsin-like properties. *J. Biol. Chem.* 286, 5967–5976.
- Szidonya, L., Cserzo, M., Hunyady, L., 2008. Dimerization and oligomerization of G-protein-coupled receptors: debated structures with established and emerging functions. *J. Endocrinol.* 196, 435–453.
- Tokaji, Z., 1993. Dimeric-like kinetic cooperativity of the bacteriorhodopsin molecules in purple membranes. *Biophys. J.* 65, 1130–1134.
- Uchihashi, T., Kodera, N., Ando, T., 2012. Guide to video recording of structure dynamics and dynamic processes of proteins by high-speed atomic force microscopy. *Nat. Protoc.* 7, 1193–1206.
- van Huizen, R., Czajkowsky, D.M., Shi, D., Shao, Z., Li, M., 1999. Images of oligomeric Kv beta 2, a modulatory subunit of potassium channels. *FEBS Lett.* 457, 107–111.
- Varo, G., Needleman, R., Lanyi, J.K., 1996. Protein structural change at the cytoplasmic surface as the cause of cooperativity in the bacteriorhodopsin photocycle. *Biophys. J.* 70, 461–467.
- Vonck, J., 1996. A three-dimensional difference map of the N intermediate in the bacteriorhodopsin photocycle: part of the F helix tilts in the M to N transition. *Biochemistry* 35, 5870–5878.
- Vonck, J., 2000. Structure of the bacteriorhodopsin mutant F219L N intermediate revealed by electron crystallography. *EMBO J.* 19, 2152–2160.
- Weik, M., Patzelt, H., Zaccai, G., Oesterhelt, D., 1998. Localization of glycolipids in membranes by in vivo labeling and neutron diffraction. *Mol. Cell.* 1, 411–419.
- Yamashita, H., Voitchevsky, K., Uchihashi, T., Contera, S.A., Ryan, J.F., et al., 2009. Dynamics of bacteriorhodopsin 2D crystal observed by high-speed atomic force microscopy. *J. Struct. Biol.* 167, 153–158.